CHAPTER 1

ENERGY AND ANGLE RECONSTRUCTION

1.1 BIGCAL CLUSTERS

Analyzer output for the BigCal is 56 by 32 matrix with energies for the each block. For energy reconstruction we first define the cluster. our Definition of the cluster is 5 by 5 matrix of the blocks surrounding most energetic block. To identify the cluster the block with maximum energy is chosen (parent block). As the next step we record the energies of blocks surrounding the maximum energy block Figure 1. 5 by 5 matrix is cut out of the BigCal and is named cluster. As the detector consists of two parts (Protvino and RSS) with different block sizes we can have mixed clusters where the matrix is not geometrically symmetric Figure 1. When cluster is identified we set the energies of the 5 by 5 matrix to 0 in main matrix (56 by 32) and repeat the procedure to obtain second, third clusters.

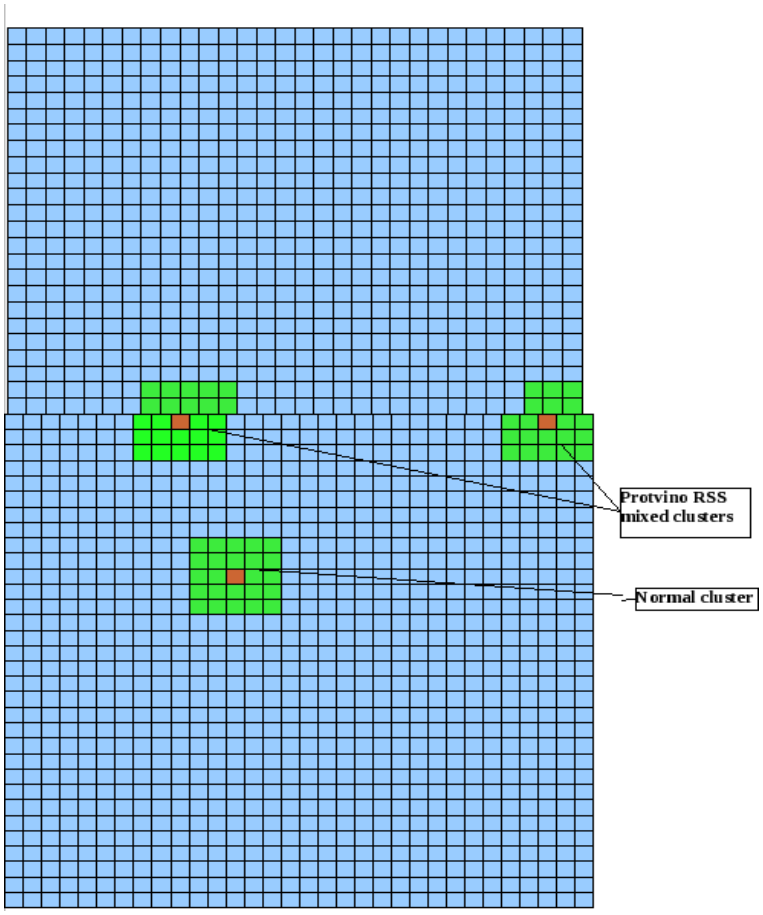

FIG. 1. BigCal cluster identification.

Also it's important to mention that several criteria were implemented for cluster identification.

- Minimal energy of the block is greater than 10MeV
- Minimal energy of parent block is 50MeV
- Minimal cluster energy is 150MeV
- Minimum number of blocks which energy greater than 10MeV in cluster greater than 2

Next challenge is correctly identify the coordinate of the cluster and energy of the cluster. The traditional methods of coordinate reconstruction Eq. 1 were failing especially when the number off cells involved was small.

$$\Delta X = \sum_i \frac{X_i/E_i^2}{1/E_i^2} \tag{1}$$

Bad coordinate reconstruction was affecting PMT gain calibration. To improve the energy resolution and coordinate reconstruction of an event we used Neural Network.

1.2 NEURAL NETWORK

During the gain calibration for BigCal we noticed that π^0 mass, reconstracted from two photon events, drifts with photon energy. The effect could come either from unexpected drift in gain parameters, from wrong coordinate reconstruction due to the conventional clustering algorithms or the complicated dependence on gain parameters. To avoid the problem with incorrect coordinate reconstruction and to take into account the cuts on minimal energy of the BigCal block we decided to use Neural Network(NN) method.

As the entry to the NN we used energy of the all 25 (5 by 5) blocks of the cluster and the parent block row iX and column iY (in 32 by 56). Using Geant simulation tool we generated six million of electrons and six million of photons to train the network. The photons were generated to obtain right calibration of the BigCal detector. The photon cluster differs from electron cluster due to effect of the magnetic field on electron and the the fact that photon shower starts about one radiation length later. The neural network was based on standard ROOT package (TMultiLayerPerceptron). NN had one hidden layer with 10 neurons and three outputs dX,dY and dE Figure 2 where dX and dY are coordinate corrections to the parent block center and dE is energy correction to the total energy of the cluster. Neuron training functions was chosen to be Gauss and learning method KBFGS. Figure 3 shows the coordinate and energy resolutions before and after corrections. Coordinate reconstruction resolution using NN showed about 3 times better results that conventional methods.

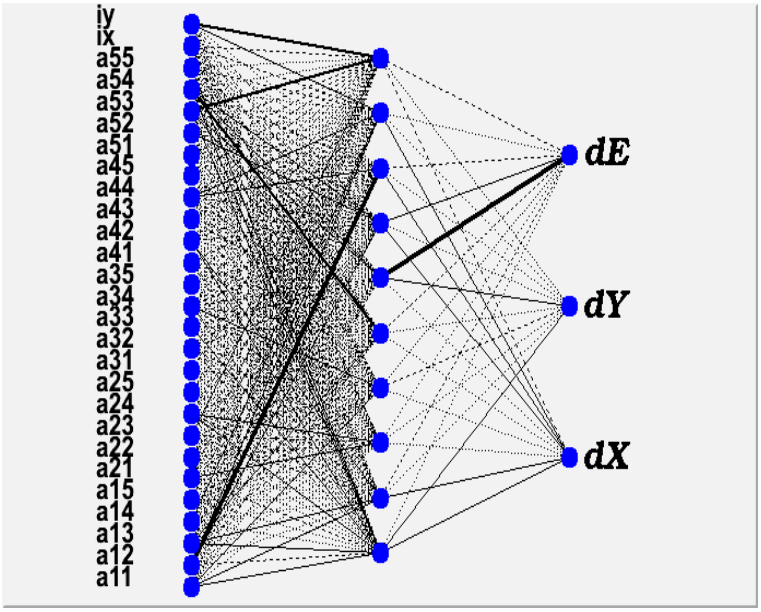

FIG. 2. Neural network structure.

We also observed that to obtain no energy dependence of the pion mass we need to use $E_{clust} = \sum E_i \dot{g}_i + \Delta E$ instead of $E_{clust} = \sum E_i \dot{g}_i$ where g_i is gain parameter for the block.

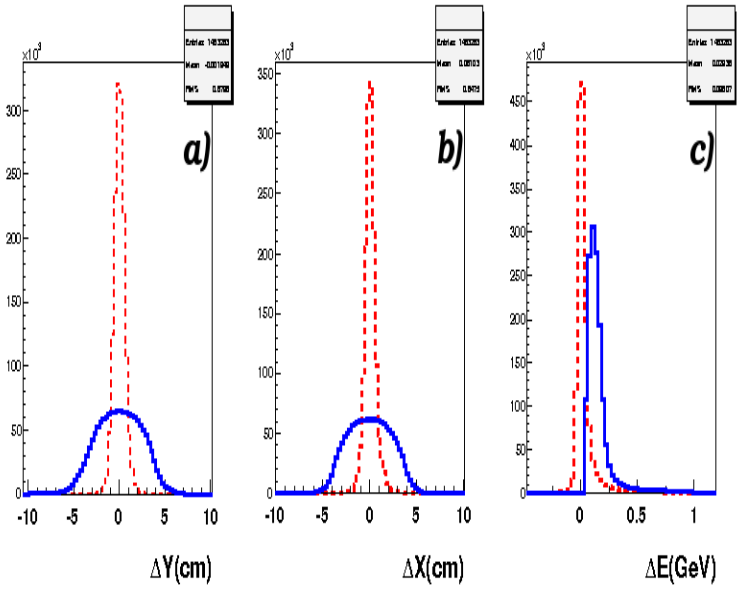

FIG. 3. Coordinate and energy resolutions before and after corrections.

1.3 POLAR AND AZIMUTH ANGLE CORRECTIONS

Neural network provided the corrected coordinates on the BigCal. Due to the magnetic field, the angles for charged particles at the target are different from angles obtained from strait line connecting the target coordinate to BigCal coordinate. To correct for the effect of magnetic field electron events were generated using GEANT simulation with different magnetic field orientations and the correction to the straight line angles was obtained using fit functions

$$(\theta_t, \phi_t) = (\theta_s, \phi_s) \cdot 180/3.1415926 +$$
$$(p_1 + p_2 \cdot \theta_s + p_3 \cdot \phi_s + p_4 \cdot \theta_s^2 + p_5 \cdot \phi_s^2 + p_6 \cdot \theta_s \cdot \phi_s) \cdot$$
$$(p_7 + p_8/E + p_9/E^2) \cdot$$
$$(p_{10} + p_{11} \cdot X_r + p_{12} \cdot X_r^2) \cdot$$
$$(p_{13} + p_{14} \cdot Y_r + p_{15} \cdot Y_r^2)$$

where θ_s, ϕ_s are angles reconstructed using straight line approximation, θ_t,ϕ_t are angles at the target, E is the energy of the cluster X_r and Y_r are raster coordinates. Figures 4,5 shows polar angle reconstruction using straight line approximation and fit procedure.Figures 6,7 shows azimuthal angle reconstruction using straight line approximation and fit procedure. Obtained angle resolutions using fit procedures are 0.5 degree for polar angle and 1 degree for azimuthal.

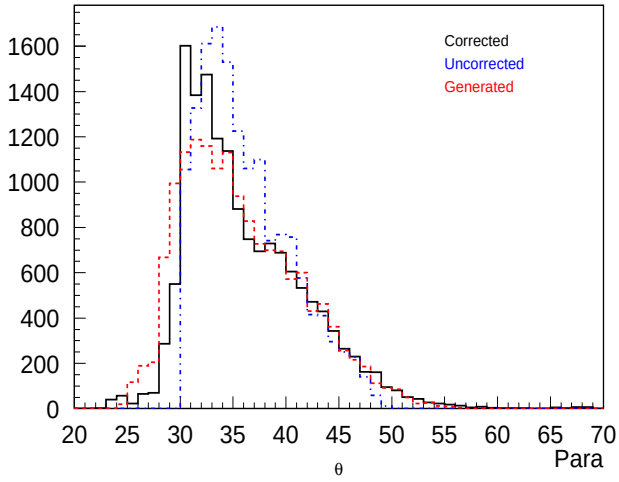

FIG. 4. Reconstruction of polar angle using fit with parallel field configuration. Red dashed line is generated spectrum, Blue dash-dotted line is reconstructed spectrum using straight line approximation, black solid line is reconstructed spectrum using fit.

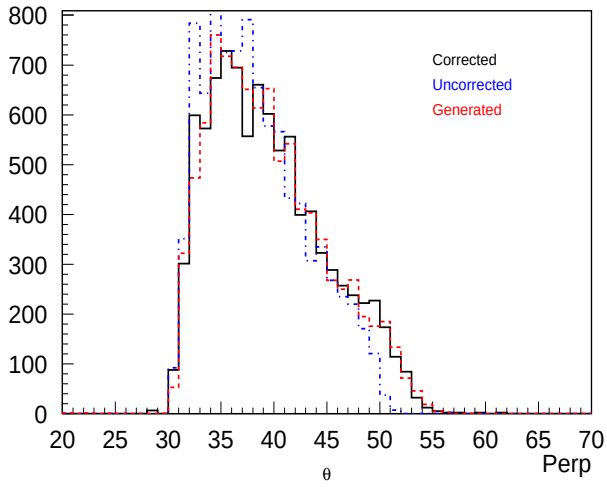

FIG. 5. Reconstruction of polar angle using fit with perpendicular field configuration. Red dashed line is generated spectrum, Blue dash-dotted line is reconstructed spectrum using straight line approximation, black solid line is reconstructed spectrum using fit.

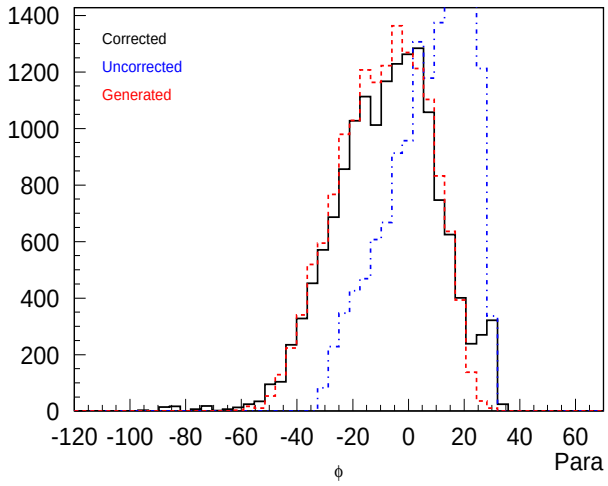

FIG. 6. Reconstruction of azimuthal angle using fit with parallel field configuration. Red dashed line is generated spectrum, Blue dash-dotted line is reconstructed spectrum using straight line approximation, black solid line is reconstructed spectrum using fit.

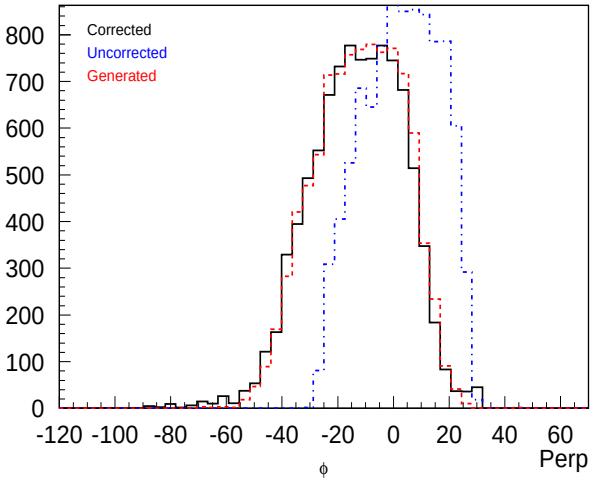

FIG. 7. Reconstruction of azimuthal angle using fit with perpendicular field configuration. Red dashed line is generated spectrum, Blue dash-dotted line is reconstructed spectrum using straight line approximation, black solid line is reconstructed spectrum using fit.

1.4 BIGCAL CALIBRATION

1.4.1 Gain Calibration

To calibrate BigCal gains we used neutral pions. The pions were selected from the sample by choosing events with two non-charged clusters(no Cerenkov). In addition we applied cuts on minimal energy of the cluster $E_{cluster} > 0.6$ GeV and number of cells in cluster with non-zero energy $N_{cell} > 4$ for better position reconstruction. Using neural network the energies of the clusters were corrected for arbitrary gain parameters and invariant mass of the events were calculated for the events. Invariant mass of the event was assigned to the most energetic block in cluster. The assumption is that the most energetic cluster is responsible for mass shift. Then the peak position was fitted and divided to neutral pion mass. The obtained parameter was chosen as next gain parameter. The procedure was repeated multiple times until the parameters brought to convergence. The neural network was crucially in obtains the correct angle and energy correction. Figure 8 illustrates the pion mass resolution obtained by this procedure. This resolution is erectly proportional to energy resolution of the clusters.

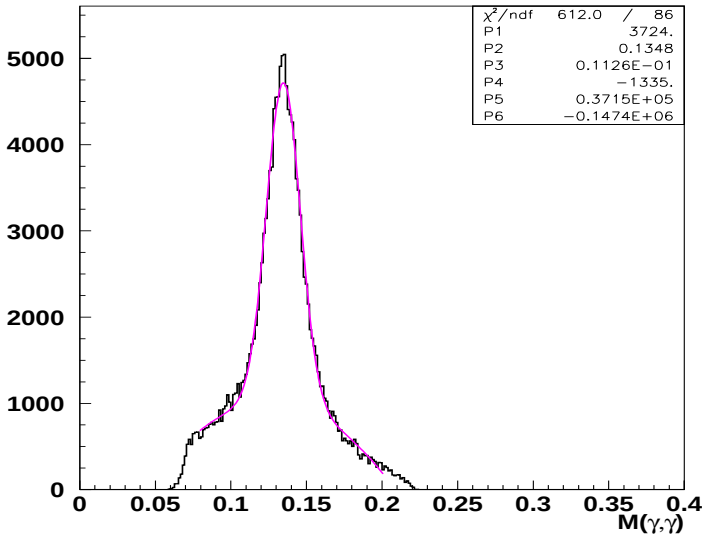

FIG. 8. Reconstructed π^0 mass from energy deposited in BigCal. An energy resolution of 8.2% has been observed.

1.4.2 Time Calibration

During the first part of the experiment BigCal was opening the trigger therefore the Čerenkov time was affected by the row of the bigcal which triggered the event. Figure 9 a) shows Čerenkov timing distribution versus triggered rows of BigCal (without correction) for one of the Čerenkov mirrors. The region corresponding to

the peaks corresponds to geometrical projection of the mirror to BigCal. To decrease the background after the cut each row was fitted with Gauss function and shifted to zero position. This procedure decreased width of one dimensional distribution. Constants were implemented into database. Figure 9 b) shows the same distribution after alignment.

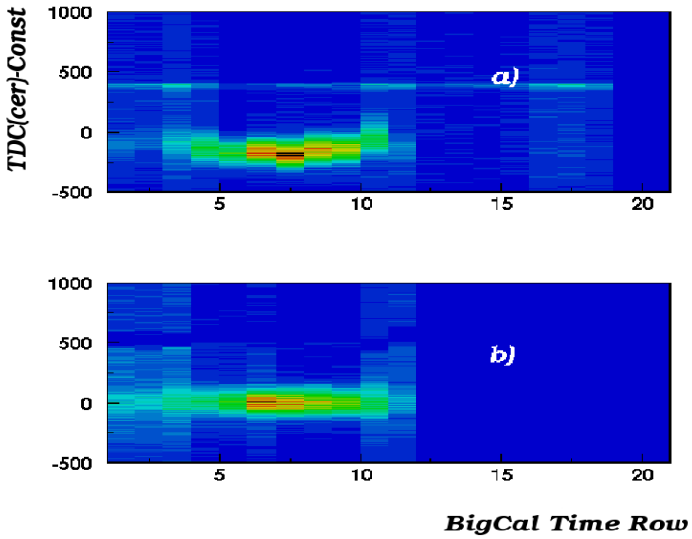

FIG. 9. Čerenkov timing peak versus BigCal triggered row a)-uncorrected, b)-corrected.

1.5 LIFE TIME CORRECTIONS

During the experiment we have lost one of the triggers information. This made impossible calculation of the life time in conventional way for positive helicity events.

$$l = \frac{N_{triggers}}{N_{scalers}} \tag{2}$$

As the solution we used the scaler and trigger information of negative helicity only. For each run we constructed the life time corresponding to negative helicity versus the number of the electrons from the number of recorded events. The distribution was parametrized using second order polynomial. Figure 10 shows the distribution of lifetime versus number of recorded triggers for negative helicity events for one of the runs. The fitted histogram is the profile of the distribution. The obtained fits were used to calculate the life time for negative and positive helicity events using

only the the number of recorded electrons. To decrease the uncertainty due to the fit, the region of the fit was set as good region. Everything out of that region are not used in the analysis. The procedure were done for each analyzed run to take into account any changes from run to run (like efficiency of the detectors, thresholds, or dead channels).

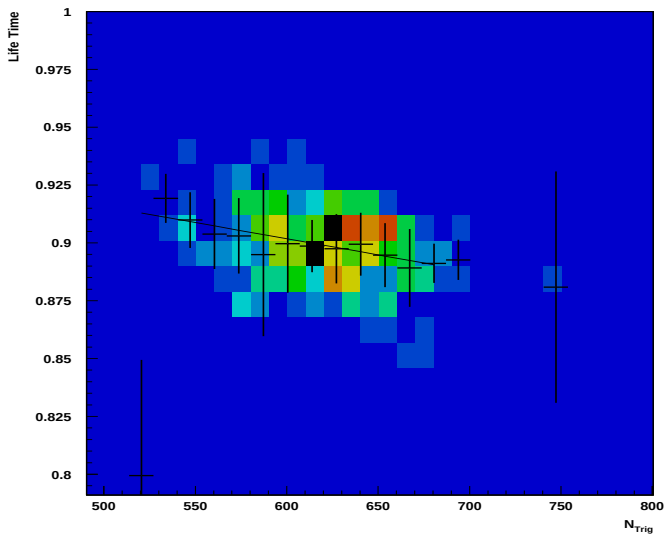

FIG. 10. Life time dependence on number of recorded triggers for negative helicity events. The fitted histogram is the profile of the distribution.

1.6 PAIR SYMMETRIC BACKGROUND

One of the important contributions to physics asymmetry comes from pair symmetric background. Neutral pions are produced inside of the target from direct electroproduction and from Bremsstrahlung spectra. These pions decay through dalitz decay and produce electron-positron (e^-,e^+) pair directly or decay into two photons which then convert to the pair. As Čerenkov detector is not able to distinguish between electrons from direct scattering and electrons originated due to pions, the calculated asymmetry is diluted by the number of electrons or positrons from pair and affected by the pair asymmetry(if any).

$$A_{calc} = \frac{N^+ - N^- + N_p^+ - N_p^-}{N^+ + N^- + N_p^+ + N_p^-} = A_{phys} \cdot d_f^p + A_{pair} \cdot (1 - d_f^p) \tag{3}$$

where

$$d_f^p = \frac{N^+ + N^-}{N^+ + N^- + N_p^+ + N_p^-} \tag{4}$$

is dilution factor originated due to the background and

$$A_{phys} = \frac{N^+ - N^-}{N^+ + N^-} \tag{5}$$

$$A_{pair} = \frac{N_p^+ - N_p^-}{N_p^+ + N_p^-} \tag{6}$$

are physics and pair asymmetry.

1.6.1 Pair symmetric Asymmetry

Pair symmetric asymmetry originates from the neutral pion asymmetry. So as the first step for the pair symmetric contribution corrections we calculated the neutral pion asymmetry using experimental data obtained from the experiment. For this purpose we used two photon events from BIGCAL to reconstruct neutral pions. Final asymmetry obtained from the data are consistent with 0.

1.6.2 Dilution due to Pair Symmetric Background

As it was mentioned above we had two major sources of pair symmetric background. The first main source was electrons-positrons originated at the target due to decay of the neutral pions (from electro and photo -production). In this case due to magnetic field we are detecting only either electron or positron the other particle is swept away from the detectors.The second source of the pair is from pair production of photons in the material out of main magnetic field. The photon are converted in the material to electron-positron pair and as the effect of magnetic field is small the pair is detected as one cluster with larger energy than in the first case.

To estimate the contribution of pair symmetric background we used epc code [2] to generate neutral pion photo and electro production at the target. Then using GEANT we propagated the decay particles through the detector setup. Obtained energy and coordinate distribution of the pair-symmetric background is not uniform due to the strong magnetic field at the target. Then we divided the BIGCAL face to 100 equal sized areas and calculated dilution factor for each side separately. Final correction is the function of coordinates at BIGCAL and energy of the cluster. Figure 11 shows fair agreement between full Monte Carlo, which includes contribution from pair-symmetric background and electroproduction, and data for different coordinate bins on BigCal.

At the same time we also checked if the number of expected neutral pions is close to experimental observation. To select pion events we used 2 cluster events with energies above 1GeV(to have almost the same condition on cluster energy cut as in experiment and to avoid issues with threshold), no Čerenkov hit for both clusters, and trigger condition (clusters should be located in different quarters of the BigCal). In addition we removed edges of the BigCal by applying cuts on $|X_{clust}| < 52$ and

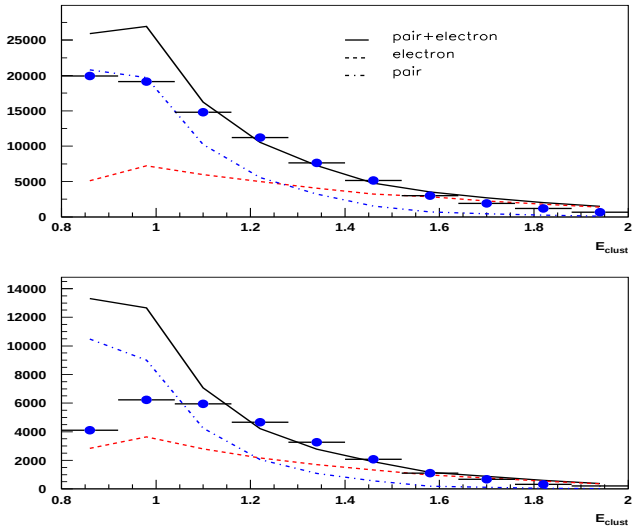

FIG. 11. Energy distribution for two different parts of BigCal. Round circles shows data, solid line shows Monte Carlo(MC) simulation of electron scattering and pair-symmetric background, dashed line shows MC simulation of electron scattering only and dash dot line shows MC simulation of pair-symmetric background only.

$|Y_{clust}| < 100$ for both clusters. We also applied the cut on number of cells in the cluster to be $N_{cell} > 4$ cells. Figure 12 shows a) Energy spectrum of generated neutral pions using two cluster reconstruction, b) Energy spectrum of the reconstructed charged particles with hit in Čerenkov , c) reconstructed neutral pions from data, d) Energy spectrum of the reconstructed charged particles with hit in Čerenkov from data. The ratio of MC pions to MC charged particles is 0.0037 while ratio for data is 0.0017. This difference can come from trigger efficiency, detector efficiency and the channels with higher thresholds. Data shows almost factor of 2 less pions than prediction from MC. The discrepancy can come from due to extra background which creates hit in Čerenkov or third cluster in BigCal.

1.7 INTERNAL RADIATIVE CORRECTIONS

Internal radiative corrections in inclusive and semi-inclusive DIS off polarized protons were performed using POLRAD 2.0 [1]. Due to lack of good experimental data in the region of interest as an input to POLRAD we used several models which are based on either current knowledge of parton distribution functions (Leader 2006, AAC) or global fit to existing data (CLAS Model) and several toy models which are based on some observations from our data. Toy models were based on distributions of $1/\nu g_1/F_1$ and $1/\nu^2 g_2/F_1$. Experimental data showed very small dependence of

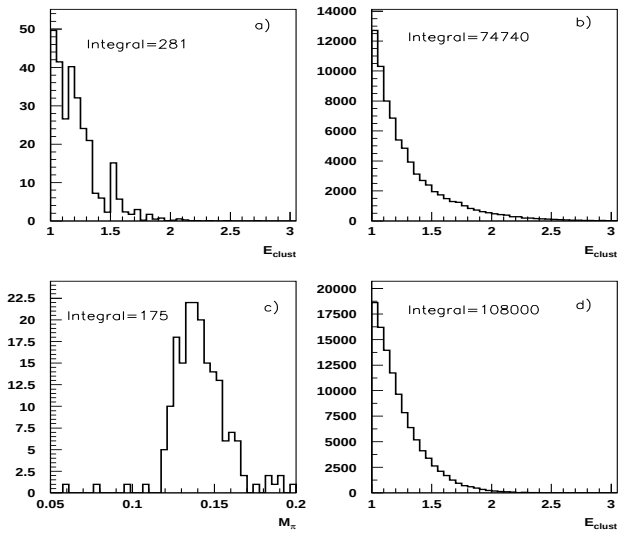

FIG. 12. Figure a) Energy spectrum of generated neutral pions using two cluster Reconstruction, b) Energy spectrum of the reconstructed charged particles with hit in Čerenkov , c) reconstructed neutral pions from data, d) Energy spectrum of the reconstructed charged particles with hit in Čerenkov from data.

$1/\nu g_1/F_1$ and $1/\nu^2 g_2/F_1$ versus $1/\nu$ distributions for different Q^2. Figure 13 shows $1/\nu g_1/F_1$ and $1/\nu^2 g_2/F_1$ obtained from data after multiple iterations with POLRAD 2.0 using toy model 0 for g_1 and and g_2. Curves represent different fits using

- g_1 Model 0 - $\frac{1}{\nu}\frac{g_1}{F_1} = \frac{1}{\nu} \cdot p_1$
- g_1 Model 1 - $\frac{1}{\nu}\frac{g_1}{F_1} = \frac{1}{\nu} * \frac{(p_1 * \frac{1}{\nu^4} + p_2)}{(p_1 * \frac{1}{\nu^4} + p_3)}$
- g_1 Model 2 - $\frac{1}{\nu}\frac{g_1}{F_1} = \frac{0.6}{\nu} * \frac{(p_1 * \frac{1}{\nu^4} + p_2)}{(p_1 * \frac{1}{\nu^4} + p_3)}$
- g_2 Model 0 - $\frac{1}{\nu}\frac{g_2}{F_1} = \frac{1}{\nu^2} \cdot p_1$
- g_2 Model 1 - $\frac{1}{\nu}\frac{g_2}{F_1} = \frac{1}{\nu^2} \cdot p_1 + \frac{1}{\nu} \cdot p_2$

which were used in different combinations to estimate systematic errors from internal radiative correction. Several iterations were performed using this models to achieve stability of the correction for A_1 and A_2. As a starting point we obtain g_1 and g_2 from fit to uncorrected data. Using the results we calculate the corrections to A_1 and A_2. Then we refit g_1 and g_2 and repeat the procedure. Figure 14 shows that A_1 and A_2 corrections converge after about 3 iterations. Figure 15 shows internal

radiative corrections to A_1 and A_2 versus Bjorken x for different models including AAC, Leader and CLAS. It is important to note that the correction to data and the uncertainty increases at low x. As final corrections we will use results obtained from CLAS fit.

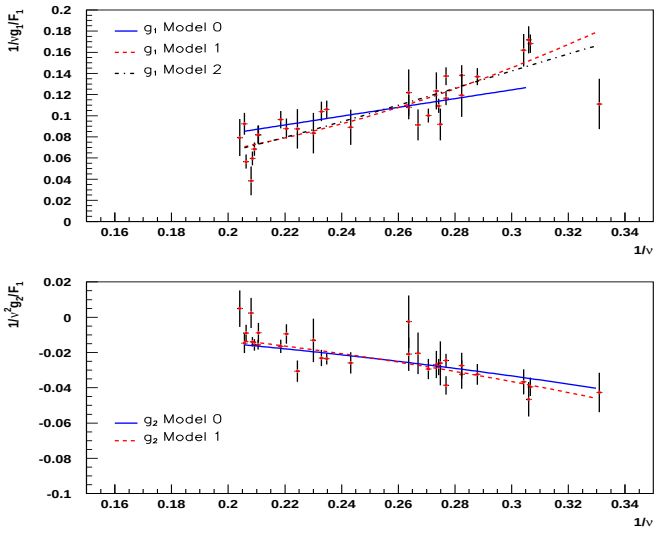

FIG. 13. $1/\nu g_1/F_1$ and $1/\nu^2 g_2/F_1$ obtained from data after multiple iterations with POLRAD 2.0 using toy model 0 for g_1 and and g_2. Curves represent different toy model fits.

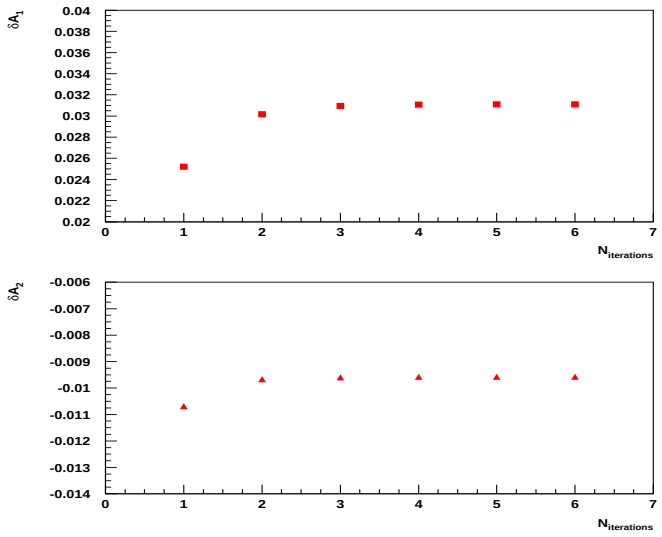

FIG. 14. A_1 and A_2 internal radiative correction versus number of iterations for one data poin using g_1 model 2 and g_2 model 0.

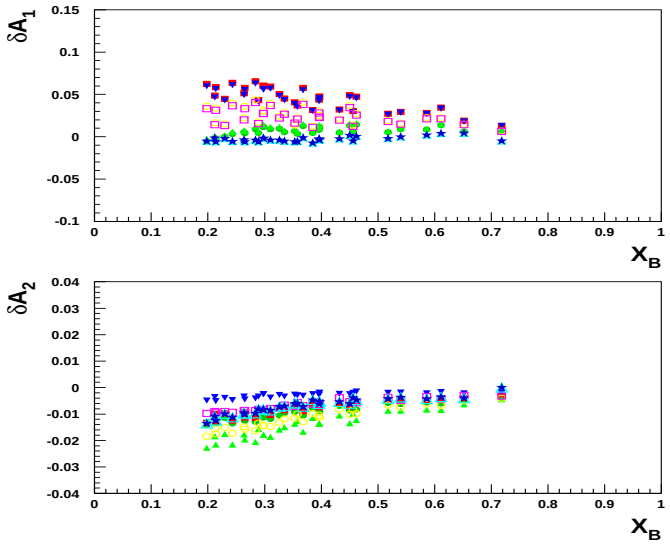

FIG. 15. A_1 and A_2 internal radiative correction versus Bjorken x.

BIBLIOGRAPHY

[1] I. Akushevich et al., Comput. Phys. Commun. 104, 201 (1997).

[2] J. W. Lightbody, J. S. O'Connell, Computers in Physics, Volume 2 Issue 3, May/June 1988